HHS Public Access

Author manuscript

Nat Chem Biol. Author manuscript; available in PMC 2016 August 01.

Published in final edited form as:

Nat Chem Biol. 2016 April ; 12(4): 218–225. doi:10.1038/nchembio.2016.

Discovery of Tumor-Specific Irreversible Inhibitors of Stearoyl CoA Desaturase

Panayotis C. Theodoropoulos[1,5], **Stephen S. Gonzales**[1,5], **Sarah E. Winterton**[1], **Carlos Rodriguez-Navas**[2], **John S. McKnight**[3], **Lorraine K. Morlock**[1], **Jordan M. Hanson**[1], **Bethany Cross**[1], **Amy E. Owen**[3], **Yingli Duan**[3], **Jose R. Moreno**[1], **Andrew Lemoff**[1], **Hamid Mirzaei**[1,4], **Bruce A. Posner**[1,4], **Noelle S. Williams**[1,4], **Joseph M. Ready**[1,4], and **Deepak Nijhawan**[1,3,4]

Joseph M. Ready: joseph.ready@utsouthwestern.edu; Deepak Nijhawan: deepak.nijhawan@utsouthwestern.edu

[1]Department of Biochemistry, UT Southwestern Medical Center

[2]Department of Molecular Genetics, UT Southwestern Medical Center

[3]Department of Internal Medicine, UT Southwestern Medical Center

[4]Harold C. Simmons Comprehensive Cancer Center, UT Southwestern Medical Center

Abstract

A hallmark of targeted cancer therapies is selective toxicity among cancer cell lines. We evaluated results from a viability screen of over 200,000 small molecules to identify two chemical series, oxalamides and benzothiazoles, that were selectively toxic to the same four of 12 human lung cancer cell lines at low nanomolar concentrations. Sensitive cell lines expressed cytochrome P450 (CYP) 4F11, which metabolized the compounds into irreversible stearoyl CoA desaturase (SCD) inhibitors. SCD is recognized as a promising biological target in cancer and metabolic disease. However, SCD is essential to sebocytes, and accordingly SCD inhibitors cause skin toxicity. Mouse sebocytes were unable to activate the benzothiazoles or oxalamides into SCD inhibitors, providing a therapeutic window for inhibiting SCD *in vivo*. We thus offer a strategy to target SCD in cancer by taking advantage of high CYP expression in a subset of tumors.

Correspondence to: Joseph M. Ready, joseph.ready@utsouthwestern.edu; Deepak Nijhawan, deepak.nijhawan@utsouthwestern.edu.

[5]These authors contributed equally to this work

Author Contributions

P.C.T., designed and performed target identification, compound selectivity, compound toxicity studies and wrote the manuscript; S.S.G., synthesized all of the benzothiazoles in the optimization that led to SW203668, Xenon-45, Alexa Fluor dye azide, and dMe-SW208108; S.E.W., synthesized all of the oxalamides in the optimization that led to SW208108; C.R.N., performed fatty acid flux analysis; J.S.M., performed molecular cloning; L.K.M., J.M.H. and B.C., performed pharmacokinetic and compound metabolism studies; A.E.O. and Y.D., assisted with compound concentration response studies; J.R.M., synthesized SW209049; A.L. and H.M., performed protein mass spectrometry; B.A.P., developed and used the S-Score analysis to identify potential selective toxins and performed unsupervised hierarchical clustering; N.S.W., designed, performed and supervised xenograft, pharmocokinetic, compound metabolism and compound toxicity studies; J.M.R., designed and supervised chemical synthetic strategies, target identification and compound toxicity studies; D.N. designed and supervised target identification, compound selectivity, compound toxicity studies and wrote the manuscript.

Competing Financial Interests

No competing financial interests declared.

Introduction

Many cancers express high levels of cytochrome P450 (CYP) mixed function oxidases[1], which, amongst other functions, metabolize xenobiotics[2]. A strategy to target toxins to cancer takes advantage of elevated CYP expression by delivering pro-drugs that are locally bio-activated into toxins[3,4]. Most CYP enzymes are also expressed in the liver, and therefore, bio-activated metabolites of the pro-drug need to be toxic to the tumor but not to the liver. For example, CYP4B1 is expressed in some non-small cell lung cancers[5] and can locally activate the molecule 4-ipomeanol into a reactive species that alkylates numerous proteins, as well as DNA, leading to cell death[3,5,6]. However, hepatic activation of 4-ipomeanol by CYP4B1 causes hepatotoxicity[5], which limits its potential as a treatment for cancer.

Here, we present a strategy for the development of CYP-activated inhibitors of the enzyme stearoyl CoA desaturase, which is not essential in the liver[7,8]. SCD inserts a double bond in the Δ9 position of saturated fatty acids. SCD is an effective cancer target because cancer cells often require *de novo* synthesis of unsaturated fatty acids to generate membranes and maintain membrane fluidity[9–11]. Small molecules that inhibit SCD are toxic to cancer cell lines, both in culture and in xenograft-derived cancer models in mice[12–15].

The clinical potential of known SCD inhibitors has been limited by mechanism-related toxicity that leads to sebocyte atrophy[16,17]. Mouse sebocytes require SCD to synthesize sebum, which is composed of esters of fatty acids and fatty alcohols. Sebum is secreted onto the skin by the hair follicles to reduce heat loss and onto the eye and eyelid by the meibomian gland for lubrication[18]. As a result, mice treated with these inhibitors have dry eye and dry skin, which leads to cold-induced hypothermia[16,17]. Accordingly, an effective SCD inhibitor for cancer therapy would need to block enzymatic function within the tumor while sparing SCD activity in sebocytes.

Here we describe two chemical scaffolds that are selectively toxic to a subset of cell lines derived from non-small cell lung cancer (NSCLC). Their selectivity is explained by differential expression of CYP4F11, which activates the compounds into potent and irreversible SCD-specific inhibitors.

Results

Small molecule screen reveals selective toxins

The UT Southwestern Center in the Cancer Target Discovery and Development Network (CTD2) screened over 200,000 compounds at a concentration of 2.5 μM on 12 different NSCLC cell lines and identified 15,483 candidate cancer toxins (Supplementary Results, Supplementary Dataset 1, Supplementary Table 1)[19,20]. We assigned a score to each compound in order to identify candidate selective toxins (Supplementary Figure 1a). Specifically, for each compound, we ranked the cell lines from most to least sensitive, and then divided them sequentially into 11 sets of two groups, designated *Sensitive* and *Resistant* (Supplementary Fig. 1b). For each set, we then calculated the difference in viability ($\Delta_{1\text{-}11}$ between the $Sensitive_{min}$ (the least sensitive cell line in the group) and $Resistant_{max}$ (the

most sensitive cell line in the group). The maximum Δ_n was assigned to each compound as the selectivity score or "S-Score". The distribution of small molecule S-Scores had two peaks (Supplementary Fig. 1c). The first peak represented compounds that were either universally toxic or non-toxic and, therefore, exhibited little variance in toxicity between cell lines. The second peak represented a skew normal distribution. We arbitrarily selected the 1,047 small molecules with S-Scores greater than 40, which represented the top 6.7% of compounds. To minimize further investigation of compounds that might be toxic to non-cancerous cells, we eliminated 499 compounds that decreased the viability of HBEC30KT[20] by more than 20% (see highlighted rows in Supplementary Dataset 1). In addition, we removed 28 compounds because there was a high degree of variance amongst the biological replicates for the sensitive cell lines[19].

Unsupervised, hierarchical clustering of the activities of the remaining 520 compounds revealed groups of small molecules with similar selectivity profiles (Supplementary Fig. 1d). Interestingly, the toxicity profile of two small molecule scaffolds clustered together in spite of chemical differences (Supplementary Fig. 1e, see highlighted rows in Supplementary Dataset 2). One scaffold, represented by 17 compounds, contained an acylated amino-benzothiazole, hereafter referred to as the benzothiazole. The other scaffold, represented by four compounds, contained an oxalic acid diamide moiety, hereafter referred to as the oxalamide.

To validate the selective toxicity of these compounds, we tested representative oxalamide SW027951 (**1**) and benzothiazole SW001286 (**2**) compounds (Supplementary Fig. 1f) for toxicity in the same 12 cancer cell lines using a concentration response study ranging from 0.3 nM to 6 μM (Supplementary Fig. 1g). For the oxalamide and the benzothiazole, the concentration that resulted in 50% less viability (IC_{50}) was less than 0.1 μM for both the H2122 and H460 cell lines. Eight of the remaining ten cell lines were insensitive to 6 μM of either compound and in two cell lines, HCC44 and HCC95, the small molecules showed intermediate toxicity. The fact that both scaffolds were toxic to the same cell lines raised the hypothesis that both compounds, in spite of their chemical differences, either affect the same pathway or share the same biological target.

To enhance the potency of these compounds while retaining cancer cell line selectivity, we synthesized approximately 100 benzothiazoles and 200 oxalamides and analyzed their activity across a subset of the lung cancer cell lines (full medicinal chemistry analysis to be published elsewhere). The medicinal chemistry optimization resulted in two lead molecules (Fig. 1a, Supplementary Fig. 1f). The optimized oxalamide, SW208108 (**3**), was toxic to four cell lines (IC_{50} 0.014 μM to 0.031 μM), intermediately toxic to one cell line (H2073, IC_{50} ~0.69 μM) and non-toxic to seven other cell lines (IC_{50} > 10 μM) (Fig 1a, b). The optimized benzothiazole, SW203668 (**4**), was selectively toxic to the same four cell lines (IC_{50} 0.022 μM to 0.116 μM) and non-toxic to the eight other cell lines (IC_{50} > 10 μM) (Fig 1a, b). The benzothiazoles, including SW203668, were more bioavailable than the optimized oxalamides (Supplementary Table 2). A pharmacokinetic analysis of SW203668 revealed plasma levels that exceeded 0.3 μM (~14-fold above the *in vitro* IC_{50}) for the first six hours and a half-life of eight hours after an intraperitoneal (IP) injection of 25 mg compound/kg body weight (Supplementary Fig. 1h).

We treated immune-deficient mice bearing 200 mm^3 tumors derived either from H2122 cells (sensitive, IC_{50} 0.022 μM) or H1155 cells (insensitive, IC_{50} > 10 μM) with 25 mg/kg of SW203668 delivered by IP injection twice a day for 10–15 days (Supplementary Fig. 1i). After the compound was administered, we observed a significantly reduced rate of growth in H2122 derived tumors. The H1155 derived tumors were unaffected, providing evidence that the selectivity and cytotoxicity of SW203668 are maintained *in vivo*.

Benzothiazoles and oxalamides target 37kDa and 30kDa proteins

The optimized oxalamide, SW208108, although unsuitable for *in vivo* studies, was ideally suited for target identification. SW208108 contains a benzophenone, which can be cross-linked to binding partners following activation by UV light. It also features an alkyne, which facilitates conjugation by copper-assisted [3+2] cycloaddition between the alkyne and azide moieties of a fluorescent dye or biotin, hereafter referred to as click chemistry[21]. Thus, we cultured sensitive (H2122) cells (SW208108 IC_{50} = 0.014 μM) in the presence of varying concentrations of SW208108 with or without exposure to ultraviolet (UV) radiation. We then subjected the resulting protein lysates to a copper-dependent click reaction in the presence of a fluorescent dye-azide conjugate. Compound-bound proteins were separated by SDS-PAGE and analyzed using a fluorescence imager. In this way, we were able to analyze both covalent (UV independent) and non-covalent (UV dependent) binding partners for SW208108.

In the absence of UV radiation, SW208108 cross-linked to proteins that migrated at both 37kDa (p37) and 30kDa (p30), reflective of covalent modification (Fig. 1c). This cross-linking was evident at 0.01 μM, which is consistent with the IC_{50} of the compound in cellular toxicity assays. Of note, we observed multiple UV dependent bands at concentrations that exceeded the IC_{50} of the probe, which suggested non-specific interactions. To determine the functional relevance of p37 and p30, we performed competition experiments wherein we co-incubated SW208108 with 10-fold excess of different oxalamide analogues representing a range of potencies. Active analogues specifically decreased the intensity of both bands, while less active ones did not (Fig. 1d). This correlation between cytotoxic activity and binding supported the hypothesis that p37 and p30 represent the biological targets for oxalamide toxicity.

The competition assay indicated that benzothiazoles also bind p37 and p30. Most strikingly, the less toxic enantiomer, (+)-SW203668 (**5**) (0.029 μM) competed for binding 6-fold less effectively than the more toxic enantiomer (−)-SW203668 (**6**) (0.007 μM, Fig. 1e, f, Supplementary Fig. 1j). We expanded this analysis by measuring binding of a panel of 30 oxalamide and benzothiazole analogues to p37 and p30. Binding to both p37 and p30 correlated with the activity of the compound with an R^2 value of 0.87 and 0.83, respectively (Fig. 1g, Supplementary Fig. 1k, Supplementary Table 3). Moreover, the EC_{50} of the p37 correlation curve was 0.31 μM, which was approximately 10-fold the IC_{50} of SW208108, consistent with our experimental conditions of a 10-fold excess of competitor. Finally, we used an alkyne-containing benzothiazole, SW209049 (**7**) (H2122 IC_{50} = 0.29 μM) to confirm that the benzothizoles also covalently modify p37 and p30 (Supplementary Fig. 1l,

m). Taken together, these results suggested that the benzothiazoles and oxalamides both act through the same target.

Benzothiazoles and oxalamides inhibit SCD

To purify p37 and p30, we treated H2122 cells with 0.1 μM SW208108 in the presence or absence of an active competitor, and clicked their lysates to a biotin-azide conjugate. We then purified biotin-modified proteins using streptavidin-conjugated beads. We resolved the purified sample by SDS-PAGE, stained with silver and, as expected, it revealed polypeptide bands at approximately 37kDa and 30kDa (Fig. 2a and Supplementary Fig. 2a). Importantly, we did not recover p37 and p30 when cells were co-exposed to 3 μM of (−)-SW203668 competitor. We excised p37 and p30 as well as corresponding gel slices from the sample that contained the competitor and identified proteins using proteomics. We ranked samples by the ratio of spectral indices between the sample with and without competitor. The highest ratio in both p37 and p30 was acyl CoA desaturase (ACOD), also known as stearoyl CoA desaturase-1 (SCD), with 28 and 13-fold competition, respectively (Supplementary Dataset 3). SCD has a predicted molecular weight of 41 kDa and a known isoform at 30 kDa that is a predicted product of alternative polyadenylation, consistent with the observed molecular weights[22].

To independently confirm that p37 and p30 are SCD, we used either rabbit IgG or SCD antibodies to immunoprecipitate proteins from SW208108-treated cell lysates. After click-mediated conjugation to Alexafluor-532 azide, we detected fluorescent p37 and p30 in the anti-SCD but not rabbit IgG precipitate (Fig. 2b and Supplementary Fig. 2b). Next, we demonstrated that a previously reported SCD inhibitor, Abbott-28c, competed with SW208108 for binding to p37 and p30 (Fig 2c, d and Supplementary Fig. 2c)[23]. Taken together, we concluded that p37 and p30 represent the two known isoforms of SCD.

SCD is a fatty acid desaturase, which introduces a *cis*-double bond in the Δ9 position of fatty acids of varying lengths[10]. *In vitro* assays for SCD activity use fatty acyl CoA substrates tritiated at the Δ9 position[24]. Desaturation at this position by SCD releases tritiated water, which can be counted to determine SCD activity. Using this assay with microsomes derived from H2122 cells, both oxalamides and benzothiazoles inhibited SCD with EC_{50} concentrations of 0.009 and 0.054 μM, respectively (Fig. 2e). These values are in the same range as their cytotoxic potencies against sensitive lines. To test whether inhibition of SCD is the cause of toxicity, we tested the efficacy of SW208108 in three different sensitive cell lines in the presence or absence of 100 μM of sodium oleate, a major product of the enzyme. Supplementation of oleate to the media fully rescued three different cancer cell lines from SW208108 toxicity (Fig. 2f). We therefore concluded that oxalamides and benzothiazoles covalently bind and inhibit SCD, which leads to cell death through depletion of unsaturated fatty acids.

Oxalamides bind and inhibit SCD only in sensitive lines

To investigate the mechanism underlying the selectivity of these agents, we compared the oxalamide to Abbott-28c in eight representative cell lines. Unlike SW208108, Abbott-28c was universally toxic to all eight cancer cell lines (IC_{50} range 0.003 to 0.015 μM) (Fig. 3a,

Supplementary Fig. 3a), indicating that SCD is essential in all cell lines. We discovered that SW208108 is only able to inhibit SCD in a subset of the cancer cell lines. Specifically, we added isotopically labeled palmitic acid ($^{13}C_{16}$-16:0) to the cells, which is elongated to stearic acid ($^{13}C_{16}$-18:0) and then de-saturated to oleic acid by SCD. Both products were expected to maintain the palmitic labeled moiety, thus, the ratio of $^{13}C_{16}$-oleic (18:1) to $^{13}C_{16}$-stearic (18:0) in lipid extracts derived from the cells would reflect SCD activity. In both H2122 and H1155 cell lines, Abbott-28c inhibited SCD in a dose-dependent fashion (Fig. 3b). By contrast, SW208108, inhibited SCD only in the sensitive cell line, H2122, but not in the insensitive cell line, H1155. We concluded that SW208108 requires a specific cellular context to inhibit SCD. Indeed, SW208108 bound SCD in the four sensitive cell lines, in the intermediately sensitive cell line (H2073) as well as in one insensitive cell line, H1993 (Fig. 3c and Supplementary Fig. 3c). In the remaining six insensitive cell lines (including H1155), SW208108 did not bind SCD. The differences in observed SCD binding could not simply be explained by differences in SCD expression (Supplementary Fig. 3b). SCD expression in H1395 and H2009 cells, for example, was nearly as high as in H2122 cells, but there was no evidence of SW208108 binding. We concluded that the ability of SW208108 to bind and inhibit SCD is context dependent and this feature underpins its selectivity. In the lone outlier, H1993, SW208108 bound p37 and p30 without causing cell death. The nature of this interaction will be discussed later.

Oxalamides are pro-drugs activated by demethylation

We reasoned that the lack of SW208108 binding to SCD in insensitive cell lines could be a consequence of compound metabolism. We therefore used LC-MS/MS to quantify the levels of SW208108 present in extracts derived from either sensitive (H2122) or insensitive (H1155) cell lines treated with the compound for various times. Surprisingly, we found that the levels of SW208108 decreased by 52% in the presence of H2122 cells after 24 hours, but remained unchanged in the presence of insensitive H1155 cells up to 48 hours (Fig. 4a). These results suggested that SW208108 represented a pro-drug and that the observed binding to p37 and p30 resulted from a metabolite that was specifically produced in sensitive cells.

When SW208108 was incubated with H2122 cells, we observed a metabolite that was 14 atomic mass units smaller than the parent drug, consistent with the loss of a methyl group (Supplementary Fig. 4a, b, c). We synthesized authentic samples of dMe-SW208108 (**8**) and determined that the concentration of dMe-SW208108 increased over time in H2122 cells treated with SW208108 but was undetectable at all time points in H1155 (Fig. 4b). Of note, the decrease in SW208108 corresponded to a stoichiometric increase in dMe-SW208108, suggesting that it was a major metabolite (Fig. 4c). Unlike SW208108, dMe-SW208108 inhibited the conversion of stearate to oleate in both H2122 and H1155 cells (Fig. 4d). Concordantly, like Abbott-28c, dMe-SW208108 was universally toxic across the eight sampled cell lines (IC_{50} range 0.003 μM to 0.015 μM) (Fig. 4e, Supplementary Fig. 4d). Taken together, we concluded that the selective toxicity of SW208108 is a consequence of selective metabolism of SW208108 to dMe-SW208108.

CYP4F11 activates oxalamides by demethylation

To identify proteins that metabolize SW208108, we focused on proteins of the cytochrome P450 family (CYP). These proteins are frequently expressed in lung epithelial cells and human NSCLC and are known to metabolize and detoxify synthetic compounds[2,25,26]. Using normalized mRNA expression data[27], we compared gene expression of CYP enzymes with the quantified p37 band (Fig. 3c), which represents the degree of SCD labeling. CYP isoforms were ranked by how well their expression levels correlated with SCD binding (Supplementary Table 4). CYP4F11 achieved the highest correlation with an R^2 value of 0.989 (Fig 5a). CYP4F11 protein expression across the original panel of 12 cell lines confirmed that it was selectively expressed in the five sensitive lines, but was not expressed in any insensitive lines (Fig. 5b and Supplementary Fig. 5f).

We used HET0016, a specific inhibitor of Cytochrome P450 4A and 4F enzymes[28], as a tool to test the role of CYP4 family members in oxalamide metabolism. The addition of HET0016 inhibited both the loss of SW208108 and the generation of dMe-SW208108 in H2122 cells (Fig. 5c). Furthermore, the addition of HET0016 inhibited the binding of SW208108 to SCD in a dose dependent fashion (Fig. 5d and Supplementary Fig. 5g). In contrast, HET0016 had no effect on the ability of dMe-SW208108 to bind SCD. Finally, HET0016 rescued the toxicity of SW208108 but not of dMe-SW208108 in H2122 cells (Fig. 5e). Taken together, these observations indicated that a CYP4 family member is necessary for SW208108 activation and, therefore, its ability to bind and inhibit SCD.

To test whether CYP4F11 is sufficient for SW208108 to bind SCD, we reconstituted SW208108 binding to SCD in HEK293T cells. HEK293T cells treated with SW208108 demonstrated no evidence of cross-linking to SCD, nor did they show any sign of CYP4F11 expression (Fig 5f and Supplementary Fig. 5h). Ectopic, transient expression of CYP4F11 produced two weak fluorescent bands, one at 37 kDa and one above 50 kDa, consistent with the endogenous SCD in these cells and the ectopic expression of CYP4F11, respectively (Fig. 5f). Consistently, SCD co-expression yielded a more intense p37 band. On the other hand, dMe-SW208108 bound SCD in the absence of CYP4F11. Finally, to test whether CYP4F11 is sufficient for SW208108 toxicity, we ectopically, stably expressed CYP4F11 in H1155 cells, which were otherwise insensitive to SW208108. In H1155 cells that ectopically expressed CYP4F11, SW208108 cross-linked SCD and was toxic (Fig 5g, 5h and Supplementary Fig. 5i). Based on the above results, we concluded that CYP4F11 de-methylates the oxalamide pro-drug unveiling dMe-SW208108, a covalent, irreversible inhibitor of SCD. Furthermore, the differential expression of CYP4F11 across cell lines explained the selective toxicity observed in our panel of lung cancer cells.

Amongst our panel of 12 cell lines, H1993 was an outlier. We observed that SW208108 cross-linked SCD in H1993 cells (Fig. 3c) even though it did not express CYP4F11 (Fig 5b) and was not sensitive to SW208108 (Fig 1b). One possible explanation is that dMe-SW208108 is generated, but either cannot inhibit SCD in H1993 or SCD is not essential to H1993. However, we found no evidence of either SW208108 metabolism or dMe-SW208108 generation in H1993 cells (Supplementary Fig. 5a). Moreover, dMe-SW208108 was toxic to H1993 cells (IC_{50} = 0.050 μM) (Supplementary Fig. 5b) demonstrating that SCD is essential in H1993 cells and dMe-SW208108 is active against this cell line.

Therefore, we concluded that the cross-linking of SW208108 in H1993 is independent of the CYP4F11-generated metabolite dMe-SW208108. We next assayed binding of other analogues to SCD using our aforementioned competition assay in H1993 cells. Interestingly, we found that unlike in H2122 cells (Supplementary Fig. 1m), the degree of competition did not correlate with analogue IC_{50} (Supplementary Fig. 5c), which suggested a different mode of binding to SCD. We tested whether this mode of binding might represent a mechanism of resistance that prevents productive SCD cross-linking by measuring SW208108 sensitivity in H1993 cells ectopically expressing CYP4F11 (Supplementary Fig. 5d). H1993 cells expressing CYP4F11 were equally sensitive to SW208108 and dMe-SW208108 ruling out a potential resistance mechanism (Supplementary Fig. 5e). Taken together, we concluded that SW208108 unproductively binds SCD in H1993. This binding may be the result of a low abundance metabolite or reflect a contextual difference in SCD. To address the latter possibility, we found no mutations in the expressed *SCD* sequence in H1993 cells, but this does not rule out cell specific post-translational modifications of SCD.

Oxalamides and benzothiazole pro-drugs spare sebocytes

Efforts to pharmacologically inhibit SCD have been limited by the toxicity of these compounds to sebocytes in the skin and other tissues[16,17]. Given that the methylated oxalamides required activation by CYP4 enzymes in order to bind SCD, we tested whether they inhibited SCD in microsomes prepared from mouse liver and preputial glands. The preputial gland is a specialized sebaceous gland and is used as a tissue source for biochemical studies of sebaceous glands[18]. We found that SW208108 inhibited SCD activity in microsomes derived from liver but not from preputial glands, whereas dMe-SW208108 inhibited SCD in both tissues (Fig. 6a). These results suggested that mouse sebocytes do not activate SW208108 *in vitro*.

This tissue-selective inhibition of SCD *in vitro* prompted us to test whether we could spare sebaceous glands *in vivo*. Because the oxalamides were not bioavailable, we first confirmed that the inhibition of SCD by benzothiazoles was also CYP4F11-dependent. Like the oxalamide, we observed that the benzothiazole alkyne SW209049 (**7**) was activated by CYP4F11 in HEK293T cells (Supplementary Fig. 6a). Furthermore, ectopic expression of CYP4F11 in H1155, an SW203668-insensitive cell line, resulted in its sensitization to toxicity by SW203668 (Supplementary Fig. 6b). These results confirmed that CYP4F11 also activates the benzothiazole, SW203668.

We compared SW203668 *in vivo* to a conventional, bioavailable SCD inhibitor developed by Xenon Pharmaceuticals, Xenon compound 45 (**9**)[29] (Supplementary Fig. 6c). Xenon-45 was cytotoxic to H2122 cells (IC_{50} = 0.095 μM) with potency similar to SW203668 (Supplementary Fig. 6d). Further, it exhibited favorable pharmacokinetic properties at 6 and 20 mg/kg, and its total levels in plasma were comparable to SW203668 in wild type (CD-1) mice (Supplementary Fig. 6e). We dosed CD-1 mice with 20 mg/kg of SW203668 or Xenon-45 once a day for two weeks after which time, skin biopsies were collected. Consistent with prior observations[17], we observed that hair follicles from Xenon-45-treated mice were devoid of sebocytes. In contrast, sebocytes were preserved in SW203668-treated

mice and their numbers were significantly higher at 20 mg/kg of SW203668 compared to 20 mg/kg Xenon-45 (Fig. 6b, c).

In an initial proof of concept experiment, we compared the anti-tumor efficacy of SW203668 versus the Xenon-45 compound by dosing immune-deficient Nod-Scid mice harboring an H2122 cell-derived tumor xenograft. Administration of 20 mg/kg of SW203668, once daily, inhibited growth of H2122 tumors, while Xenon-45 displayed no efficacy at this dose (Supplementary Fig. 6f). We concluded that SW203668 is less toxic than Xenon-45 and has more efficacy, revealing a wider therapeutic window. Both compounds displayed significantly more sebocyte toxicity in the skin of Nod-Scid tumor-bearing mice than what was seen in wild type mice (6 mg/kg Xenon-45 in Nod-Scid mice versus CD-I mice; p-value = 0.0496, one-tailed t-test, n=3 biological replicates). As a result, in Nod-Scid mice, the SW203668 therapeutic index was evident at a lower dose, 6 mg/kg (Supplementary Fig. 6g). This shift may be attributable to a strain difference.

Finally, we explored whether CYP enzymes other than CYP4F11 are capable of activating the oxalamides and benzothiazoles. We co-expressed SCD and nine different type-4 CYPs in HEK293T cells and evaluated cross-linking of SCD by the oxalamide and benzothiazole pro-drug alkynes, SW208108 and SW209049. Indeed, several members of the CYP4 family were capable of activating these compounds, including CYP4F11, CYP4F12, CYP4F22 and CYP4V2 (Fig. 6d and Supplementary Fig. 6h). Based on data from The Cancer Genome Atlas (TCGA)[30], this set of four CYP enzymes is expressed at high levels relative to matched normal tissue in a diverse set of cancers, with each CYP isoform occurring in up to 15% of samples (Fig. 6e, Supplementary Table 5).

Discussion

Cells require unsaturated fatty acids (UFAs) obtained either by *de novo* synthesis from SCD or through uptake from their environment for membrane synthesis and proliferation[9_11]. Hence, SCD is essential in proliferating cancer cells conditional on the exogenous supply of UFAs, therefore, inhibition of SCD leads to depletion of UFAs and cell death. A major obstacle for targeting SCD in cancer has been the toxicity of systemic SCD inhibitors to sebocytes. Other than this, no other serious toxicity has been identified by whole body inhibition of SCD, either by systemic inhibitors or in mice lacking the major SCD isoform[7,16,31]. Our pro-drug SCD inhibitors did not inhibit SCD in sebaceous glands *in vitro*, and spared sebaceous glands *in vivo* at doses that significantly inhibited tumor growth.

Interestingly, a canonical SCD inhibitor, Xenon-45, had lower anti-tumor efficacy than the benzothiazoles but exhibited greater skin toxicity. The site-specific activation of the benzothiazole might lead to higher levels of the active compound in the tumor. Alternatively, the irreversible binding of the benzothiazoles might maintain enzyme inhibition even after the parent compound is cleared from the animal.

Unlike 4-ipomeanol, which is activated by CYP4B1 into a reactive alkylating agent[3], dMeSW208108 was chemically stable. Based on our SDS-PAGE analysis of cross-linked proteins, with or without UV illumination, we observed specific binding to SCD relative to

other proteins. Furthermore, oxalamide and benzothiazole toxicity was fully rescued by oleate, suggesting that the cytotoxicity was solely due to SCD inhibition.

A major challenge of utilizing CYPs to activate cancer toxins is the concomitant hepatoxicity, because the liver expresses most CYP enzymes. Importantly, mice with a liver-specific SCD knockout are viable[7] and SCD inhibitors do not display hepatotoxicity in mice. In addition, Merck tested a liver-targeted SCD inhibitor in phase 2 clinical trials and did not observe liver toxicity[8]. However, at higher concentrations of the benzothiazole we did observe sebocyte toxicity. One likely explanation is that metabolism of the benzothiazole by the liver leads to increased plasma levels of the active metabolite. In the future, optimized molecules in which active metabolites are not secreted into the plasma might show an even greater therapeutic index.

Liver-specific targeting of SCD has been the subject of considerable attention for its beneficial metabolic effects. Tissue specific deletion of SCD1 in mouse liver results in impaired glycogen and glucose synthesis but also prevents carbohydrate induced adiposity and fatty liver[7]. We found that the oxalamides inhibited SCD in liver microsomes. Therefore, liver-specific inhibition of SCD for the treatment of fatty liver disease represents another potential application of these compounds.

Because covalent interactions of oxalamides and benzothiazoles were specific to CYP4F11 and SCD, we hypothesize that there is a shared feature of the SCD and CYP4F11 active sites, which accommodates these molecules and renders them locally reactive. Binding of the oxalamides could be competed away by a known, presumably non-covalent, SCD inhibitor, suggesting that oxalamides bind and react in the active site of SCD. Both SCD and CYP4F11 are iron-containing ER membrane proteins that can hydroxylate fatty acid substrates[32–35]. The similar substrate specificity and chemistry of these two enzymes is likely to be relevant to the activation of these compounds. Co-crystallizing the enzyme in complex with the oxalamides and benzothiazoles could be the subject of a future investigation to shed light on the precise mode of binding of these irreversible SCD inhibitors[36,37]. Systematic screening of CYPs and other enzymes for the ability to activate oxalamides and benzothiazoles could also be the subject of a future investigation that seeks to define a more comprehensive set of tumor biomarkers for these compounds.

Online Methods

Experimental Reproducibility

All experiments with the exception of animal experiments were replicated at least twice. Animal experiments used multiple biological replicates determined by a power calculation, which is described in detail in a later section.

High Throughput Screening

See Supplementary Table 1 for a description of assay format and screening procedures.

S-Score Analysis

For the application of the S-score method described in the main text, the activity of each compound against each cell line was expressed as the median of three replicates. The S-score script was implemented in Perl (version 5.22.0) and is shown below:

```
#!/usr/bin/perl -w
open(INS, “input.txt”); open(OUT, “>output.txt”); @a=<INS>; close INS; for
($t=0;
$t<@a; $t++) {chomp $a[$t]; @b=(); @b=split(/ /, $a[$t]); @c=(); @c=sort
{ $a <=>
$b } @b; $j=0; @delta=(); for ($s=1; $s<@c; $s++) {$delta[$j]=($c[$s]-
$c[$s-1]);
$j++;}@d=(); @d=sort { $b <=> $a } @delta; $k=0;for ($ss=0; $ss<@delta; $ss+
+) {if
($delta[$ss]==$d[0]){$k=$ss; last;}}
$kk=($k+1); print OUT $delta[$k], “”; print OUT $kk, ””; print OUT “\n”;}
close OUT;
```

Unsupervised, hierarchical clustering

The results from rescreening of the 15,483 compounds which were toxic to at least one of the NSCLC cell lines were clustered using the unsupervised hierarchical clustering algorithm available in Spotfire (version 6.5.3; Tibco, Inc. licensed through Perkin-Elmer, Inc.). The clustering utilized the unweighted pair-group method with arithmetic mean (UPGMA) and the Euclidean distance measure. Additional details can be found in the manufacturer’s user manual and the Perkin-Elmer/Tibco website (http://www.cambridgesoft.com/ensemble/spotfire).

Cell culture and compound concentration responses

All NSCLC cell lines were obtained from the Minna and Gazdar laboratory at UT Southwestern Medical Center. They were screened for mycoplasma and authenticated by short tandem repeat (STR) analysis through the McDermott Core at UT Southwestern. All NSCLC cell lines were cultured in RPMI 1640 (Sigma) supplemented with 5% fetal bovine serum (FBS) (Sigma) and 2mM L-Glutamine (Sigma). HEK293T cells were cultured in DMEM supplemented with 10% FBS and 2 mM L-glutamine. For concentration responses, cells were plated in 96-well plates at 15% confluence in 100 μl of the above media and were allowed to settle overnight. On the next day, this medium was removed and new medium containing a 10-point concentration response was added, starting from 6 μM and decreasing in 3-fold serial dilutions in DMSO. The final concentration of DMSO in each well was 0.5%. Each dose of compound was tested in duplicate and the values displayed represent the average of these duplicates.

Compound Treatment, cell lysis and click chemistry

Cells were plated in 6-well plates at 100,000 cells per well and were allowed to adhere overnight. The next day, the media was replaced with the relevant concentration of compound, diluted from a concentrated DMSO stock 1:1000. All compound treatments were for 2h at 37 °C and 5% CO_2. For UV cross-linking, cells were placed on ice approximately 3–4 inches below the bulbs in a stratalinker and then exposed to 15 minutes of UVB radiation. The media was removed and the cells were immediately solubilized in 1% SDS, with benzonase (Sigma #E1014) diluted 1:10,000 in Buffer A (50 mM HEPES 7.4, 10 mM KCl, 2 mM $MgCl_2$). Lysates were protein normalized using the BCA assay (Life Technologies #23227) and subjected to a click reaction with 100 μM TBTA (dissolved in 4:1 DMSO:t-butanol), 1 mM TCEP, 2 mM $CuSO_4$ and 25 μM Alexafluor-532 azide **(10)** (see supplementary compound procedures for synthesis) for 1 h at 25°C with agitation. SDS sample buffer was then added to the samples to quench the reaction, and proteins were resolved by SDS-PAGE. A typhoon scanner with a 532 nm excitation laser and a 555 nm emission filter was used to scan the gels for fluorescently labeled proteins.

Purification of compound-bound proteins

Cells were treated with the relevant compounds as described above but on a larger scale, in 15 cm Petri dishes, in order to obtain 100 mg of protein lysate per purification condition. Lysates underwent a click reaction with 100 μM TBTA, 1 mM TCEP, 2 mM $CuSO_4$ and 100 μM diazo biotin azide (Click Chemistry Tools #1041-25) for 1 hour at 25 °C. Proteins were then precipitated with 4 volumes of cold acetone, and the insoluble protein pellets were spun down at 6,000g and resolubilized in 4% SDS and 7M urea in PBS overnight. Insoluble material was collected by centrifugation at 20,000g and lysates were filtered at 0.45 μm and at 0.22 μm. Streptavidin agarose beads (Solu-link #N-1000-010) were then added and incubated with the resolubilized protein for 1 hour at 25 °C. The beads were washed three times with 4% SDS in PBS and the protein was eluted at 95°C in Laemmli sample buffer. Proteins were resolved by SDS-PAGE, and the gel was stained with silver (Pierce #24612). The relevant bands were excised and destained.

Proteomic Analysis

Protein in gel bands were digested overnight with trypsin (Promega) following reduction and alkylation with DTT and iodoacetamide (Sigma). Following solid-phase extraction cleanup with Oasis HLB plates (Waters), the resulting samples were reconstituted in 10 μl of 2% (v/v) acetonitrile (ACN) and 0.1% trifluoroacetic acid in water. 2 μl were injected and analyzed by LC/MS/MS using an Orbitrap Elite mass spectrometer (Thermo Electron) coupled to an Ultimate 3000 RSLC-Nano liquid chromatography system (Dionex). Samples were injected onto a 75μm i.d., 50-cm long Easy Spray column (Thermo) and eluted with a gradient from 1–28% of buffer D in buffer C over 60 min at 250 nl/min flow rate. Buffer C contained 2% (v/v) ACN and 0.1% formic acid in water, and buffer D contained 80% (v/v) ACN, 10% (v/v) trifluoroethanol, and 0.08% formic acid in water. The mass spectrometer operated in positive ion mode with a source voltage of 2.2 kV, capillary temperature of 250°C, and S-lens RF level at 60.0%. MS scans were acquired at 240,000 resolution and up to 14 MS/MS spectra were obtained for each full spectrum acquired using collisionally

induced dissociation (CID) for ions with charge ≥2. Raw MS data files were converted to a peak list format and analyzed using the central proteomics facilities pipeline (CPFP), version 2.0.3 [38]. Peptide identification was performed using the X!Tandem[39] and open MS search algorithm (OMSSA)[40] search engines against the human protein database from Uniprot, with common contaminants and reversed decoy sequences appended[41]. Fragment and precursor tolerances of 20 ppm and 0.5 Da were specified, and three miscleavages were allowed. Carbamidomethylation of Cys was set as a fixed modification and oxidation of Met was set as a variable modification. An additional requirement of two unique peptide sequences per protein was used for protein identification.

Western blots

Proteins were resolved via SDS-PAGE and transferred to 0.5 μm nitrocellulose membranes. Membranes were blocked in 5% milk TBST for 5 minutes and then primary antibodies were added in 5% milk and incubated on a shaker overnight at 4°C. HRP-conjugated antibodies, including secondary antibodies and anti-tubulin-HRP were incubated for 1 hour at room temperature. The following antibodies were used: anti-SCD (1:1000, Pierce #PA5-19682), anti-CYP4F11 (1:500, Santa Cruz, sc-53619), anti-tubulin-HRP (1:10,000, Protein Tech #HRP66031), and anti-V5-HRP (1:5000, Sigma #V2260).

Immunoprecipitation and click chemistry

Protein was extracted with 1% NP-40 Buffer A from SW208108-treated H2122 cells. 1 μg of SCD antibody (Pierce #PA5-19682) or rabbit IgG (Cell Signaling #2729) was added to 500 μg of lysate. Protein-antibody complexes were pulled down with protein A/G beads (Santa Cruz #sc-2003) and were washed with lysis buffer. Buffer A with 1% SDS containing click reagents and the fluorescent dye-azide was added to the beads. After 1 hour, the beads were spun down and Laemmli buffer was added to the supernatant, which was run on SDS-PAGE and scanned as described above.

SCD *in vitro* assay

We modified previously described procedures[24] in the following way. Reactions were performed in 200 μl with 50 μM of stearoyl [9,10-3H] Coenzyme A (American Radiolabeled Compounds, #ART 0390-50 μCi) in Buffer A. Microsomes were used for all samples and prepared as follows. Cells or tissues were lysed in Buffer A using a syringe or dounce homogenizer, respectively, and centrifuged at 1,000g. The resulting supernatant was centrifuged at 100,000g and the pellet was resuspended in Buffer A yielding the microsomal fraction. For SCD activity assays of H2122, liver and preputial glands, 800, 200 and 1,000 μg of protein were used, respectively. Microsomes were first incubated with the relevant compound at 37°C for 15 minutes with 1 mM NADPH (Sigma #N7505), then stearoyl [9,10-3H] Coenzyme A was added to 50 μM and NADPH was increased to 2 mM. The reactions were allowed to incubate at 37°C for 30 minutes. Then 300 μl cold Buffer A was added and the suspensions were transferred to 100 mg charcoal, mixed briefly. The charcoal was removed by centrifugation at 20,000g. The supernatants were filtered and 200 μl were added to 10 ml of scintillation fluid.

Fatty acid flux analysis

Cells were incubated with 10 μM $^{13}C_{16}$ palmitate (Sigma #605573) for 4 hours at 37 °C. Total fatty acids extracted from approximately 500,000 cells were quantified using GC-ECNI-MS in triplicate as previously described[42]. Basic hydrolysis of lipid extracts was performed as described[43] for the quantification of pooled free and esterified fatty acids. SCD activity was demonstrated by the quantification of the isotopic m/z ions containing +16 units of mass (from labeled $^{13}C_{16}$-palmitate used as substrate). To avoid misinterpretation due to the excess of remaining $^{13}C_{16}$-palmitate from the cell culture media, we present the flux ratio of ^{13}C labeled oleic to stearic acid.

Expression data

Expression data for the CYP enzymes was obtained from the Cancer Cell Line Encyclopedia (CCLE)[27]. Expression data was available only for eight of the 12 NSCLC cell lines, all of which have been displayed herein.

Plasmids

SCD cDNA was amplified from U2OS cDNA library (5′ ATGATGGAATTCCACCGCCatgccggcccacttgctgcagga; 5′ ATGATGGGATCCtcagccactcttgtagtttcc) and cloned into pLVX-IRES-Puro (Clontech) using EcoRI and BamHI. CYP4F11 cDNA used in Fig. 5 and Supplementary Fig. S6a was obtained from Open Biosystems (Clone ID: 3846027), was PCR-amplified using the following primers (5′ ATGATGTCTAGAATGCCGCAGCTGAGCCTGTCCTGGC; 5′ ATGATGGCGGCCGCTCACTGTGAGTTCGCACCCAGGGGCTC) and then cloned into pLVX-IRES-Puro (Clontech) using XbaI and NotI. For Fig. 6d, all CYP cDNAs were obtained from the Invitrogen Ultimate ORF Library Collection in Gateway entry vectors and were cloned into pLX302 (Addgene #25896) using an LR reaction (Life Technologies). In all of the resulting plasmids, the stop codon was mutated to glycine to allow for translation of a short linker followed by a V5 epitope. The primers used for site directed mutagenesis are the following: CYP4A11 (5′ CTCAGGAGGATCAAGGGGGAACCCAGCTTTCTTG and 5′ CAAGAAAGCTGGGTTCCCCCTTGATCCTCCTGAG, CYP4V2 (5′ GAAATGCAGATGAACGCGGGAACCCAGCTTTCTTG and 5′ CAAGAAAGCTGGGTTCCCCCTTGATCCTCCTGAG), CYP4F22 (5′ CTGCCTCCGCGGGCCGGGAACCCAGCTTTCTTG and 5′ CAAGAAAGCTGGGTTCCCGGCCCGCGGAGGCAG), CYP4X1 (5′ GAAACTCTCTGAATGTGGGAACCCAGCTTTCTTG and 5′ CAAGAAAGCTGGGTTCCCACATTCAGAGAGTTTC), CYP4F11 (5′ GTGCGAACTCACAGGGGAACCCAGCTTTCTTG and 5′ CAAGAAAGCTGGGTTCCCCTGTGAGTTCGCAC), CYP4B1 (5′ CTGGGTCTGGGAAGGGGAACCCAGCTTTCTTG and CAAGAAAGCTGGGTTCCCCTTCCCAGACCCAG), CYP46A1 (5′ CACCACCCCCCTGCGGGAACCCAGCTTTCTTG and 5′ CAAGAAAGCTGGGTTCCCGCAGGGGGGTGGTG), CYP4F12 (5′ GAATGTAAGCTTGCAGGGGAACCCAGCTTTCTTG and 5′ CAAGAAAGCTGGGTTCCCCTGCAAGCTTACATTC), CYP4Z1 (5′

CAAAAAAAGTTTGCGGGAACCCAGCTTTCTTG and 5′ CAAGAAAGCTGGGTTCCCGCAAACTTTTTTTG).

Lentiviral packaging and infection

Lentivirus was generated from pLVX-IRES-Puro and pLVX-IRES-Puro-CYP4F11 by transfecting Lenti-X HEK293T (Clontech) cells with the Fugene HD reagent (Promega #E2312) using the three-vector system, as decribed[44]. Infections were performed by co-treatment of virus and 8 μg/ml polybrene and after 1d were subjected to 2 μg/ml puromycin selection.

Reconstitution of SCD crosslinking in HEK293T cells

For HEK293T cross-linking reconstitution experiments, 300ng of each plasmid or empty vector was transfected into HEK293T cells in 6-well plates using the Fugene HD reagent (Promega #E2312). Complexes were removed after 5 hours and compound treatments were performed 2 days later. Compound treatments, lysate preparation, western blots and click reactions were then performed as described above.

Animals

Male and female CD-1 mice at 5–7 weeks of age were obtained from Charles River Laboratories (Wilmington, MA). Male and female Nod-Scid mice at 6–8 weeks of age were obtained from the Mouse Breeding Core at UT Southwestern Medical Center. All animal experiments were performed without randomization or blinding. All animal protocols were reviewed by the Institutional Animal Care and Use Committee before studies commenced. The Animal Resource Center at UTSW is accredited by the American Association of Accreditation of Laboratory Animal Care (AAALAC) and follows standards set forth in the Guide for Care and Use of Laboratory Animals. This institution is in full compliance with the Animal Welfare Act.

Analytical LC-MS/MS conditions

SW208108, dMe-SW208108 and SW203668 compound levels for metabolic stability and pharmacokinetic studies were monitored by LC-MS/MS using an AB Sciex (Framingham, MA) 4000 Qtrap mass spectrometer coupled to a Shimadzu (Columbia, MD) Prominence LC. All three analytes were detected with the mass spectrometer in positive MRM (multiple reaction monitoring) mode by following the precursor to fragment ion transition 457.186 to 135.1 for SW208108, 443.252 to 121.0 for dMe-SW208108 and 390.13 to 210.1 for SW203668. An Agilent C18 XDB column (5 micron, 50 × 4.6 mm) was used for chromatography for all three compounds with the following conditions: Buffer E: dH20 + 0.1% formic acid, Buffer F: methanol + 0.1% formic acid, 0–1.5 min 3% F, 1.5 – 2 min gradient to 100% F, 2 – 3.2 min 100% B, 3.2 – 3.5 min gradient to 3% F, 3.5 – 4.5 3%. N-benzylbenzamide (transition 212.1 to 91.1) or tolbutamide (transition 271.2 t0 91.2) both from Sigma (St. Louis, MO) were used as internal standards (IS).

S9 metabolic stability

For S9 studies, 2 μM of each compound was incubated in a 0.5 ml incubation volume with 0.5 mg (1 mg/ml) of murine CD-1 S9 (combined cytosol and microsome) fractions purchased from Celsis/In Vitro Technologies (Baltimore, MD) and Phase I (an NADPH regenerating system) cofactors (Sigma) for 0–240 min. Reactions were quenched by mixing the incubation mixture with an equal volume of methanol containing formic acid and the N-benzylbenzamide or tolbutamide internal standard. The quenched mixture was vortexed for 15 sec, incubated at room temperature for 10 min and spun for 5 min at 986g. Supernatants were then transferred to an Eppendorf tube and spun in a refrigerated microcentrifuge for 5 min at 16,100g. The second supernatant was transferred to an HPLC vial and analyzed by LC-MS/MS. Transitions used to monitor compound levels in MRM mode are listed in Supplementary Table 2. Chromatography conditions were similar to those listed for SW203668, dMe-SW203668 and SW208108. Metabolic stability studies using both Phase I and Phase II (UDPGA and PAPS both from Sigma) cofactors were conducted similarly. Metabolism of 7-ethoxycoumarin was used to monitor S9 performance. We used the previously described method[45] with modification for determination of metabolic stability half-life by substrate depletion. A “% remaining” value was used to assess metabolic stability of a compound over time. The LC-MS/MS peak area of the incubated sample at each time point was divided by the LC-MS/MS peak area of the time 0 (T0) sample and multiplied by 100. The natural Log (ln) of the % remaining of compound was then plotted versus time (in min) and a linear regression curve plotted going through the y-intercept at ln(100). The metabolism of some compounds failed to show linear kinetics at later time points, so those time points were excluded. The half-life (T ½) was calculated as T ½ = −0.693/slope. If a negative slope was not observed (no compound loss over time), T ½ is indicated as >240 min, the last time point evaluated.

Determination of compound stability in cell lines

H2122 and H1155 cells were plated at a density of 2,000 cells per well in 96 well plates. After overnight adherence, media was removed and replaced with fresh media containing 100 nM SW208108 +/− the CYP4A and 4F inhibitor, HET0016. The plates were incubated at 37°C, 5% CO_2. At varying times post compound addition, media and cells were lifted and a two-fold volume of methanol containing 0.2% formic acid and 100 ng/ml of internal standard (N-benzylbenzamide) was added followed by vigorous vortexing and centrifugation at 16,000g for 5 min. The supernatant was analyzed by LC-MS/MS for levels of parent SW208108 and demethylated SW208108 (dMe-SW208108). Compound levels were quantitated in reference to standard curves prepared by adding varying concentrations of SW208108 and synthetic dMe-SW208108 to untreated blank H2122 and H115 lysates and processing as described above.

In vivo toxicity studies

Male 6-week-old CD-1 mice were dosed once daily for 15 days with either SW203668 at 6 and 20 mg/kg intraperitoneal (IP) injection in 10% DMSO, 10% Cremophor EL (Sigma), 80% 50 mM lactic acid, pH 5.5, or Xenon-45 at 6 and 20 mg/kg administered per os (PO), i.e. orally, in 1% carboxymethylcellulose/10% PG/0.1% Tween 20. Male mice were used in

order to allow the option of collecting preputial glands for further experiments but they were not utilized in this study. Mice were weighed and visually inspected each day. Three hours after the 15th and last dose, animals were euthanized, blood was collected for evaluation of compound levels, and skin was collected for histological evaluation of compound effects on sebocytes.

Pharmacokinetic studies

Pharmacokinetic studies were performed by injecting 6–7 week old CD-1 female mice with SW203668 at 25 mg/kg IP formulated in 10% DMSO, 10% Cremophor, 80% 50 mM lactic acid, pH 5.5. Female mice were used for greater ease of maintenance and handling. Animals were sacrificed in groups of three, blood was obtained by cardiac puncture at each time point (0, 10, 30, 90, 180, 360, 960 and 1440 min post dose) using the anticoagulant acidified citrate dextrose, and plasma was isolated by centrifugation. 100 μl of plasma was mixed with 200 μl of methanol containing 0.15% formic acid and 20 ng/ml N-benzylbenzamide IS. The samples were vortexed 15 sec, incubated at room temp for 10′ and spun twice at 16,100g at 4 C in a refrigerated microcentrifuge. The amount of SW203668 present in plasma was quantified by LC-MS/MS to determine the rate of clearance from mouse blood. Standard curves were generated using blank plasma (Bioreclamation, Westbury, NY) spiked with known concentrations of SW203668 and processed as described above. The concentrations of SW203668 in each time-point sample were quantified using Analyst 1.6.1. A value of 3-fold above the signal obtained from blank plasma was designated the limit of detection (LOD). The limit of quantitation (LOQ) was defined as the lowest concentration at which back calculation yielded a concentration within 20% of theoretical. Pharmacokinetic parameters were calculated using the noncompartmental analysis tool of Phoenix WinNonLin (Certara/Pharsight, Sunnyvale, CA). Plasma levels of SW203668 dosed IP daily at 6 and 20 mg/kg and of Xenon-45 dosed PO at 6 and 20 mg/kg in 1% CMC/10% PG/0.1% Tween 20 for 15 days in wild type and tumor bearing Nod-Scid mice were determined similarly.

Xenograft experiments

To determine the group size for xenograft experiments, we defined a response as a 50% reduction in tumor volume in the range of linear growth of a subcutaneous xenograft (up to ~800 mg). Using a power analysis (Sigma Plot, ANOVA) with an expected difference in tumor volumes of 400 mg (50% of control) and standard deviations in measurements of +/− 200 mg, then a power analysis indicates that a group size of eight will provide 90% power to detect a 50% difference with an alpha of 0.05. Therefore, all xenograft experiments used a group size of at least eight mice. Male and female Nod-Scid mice were injected with 5×10^6 H2122 or H1155 cells by subcutaneous injection in a single site on their left flank. When tumors reached approximately 150–200 mm^3, the animals were randomized into groups of either 12 mice (Supplementary Fig. 1) or 8 mice (Supplementary Fig. 6). In the first experiment, mice bearing either H2122 tumors or H1155 tumors were dosed IP twice daily for 15 days at 25 mg/kg with SW203668 formulated as previously described or with vehicle. In the second experiment, H2122 tumor- bearing mice were dosed once daily with either 6 or 20 mg/kg SW203668 IP or 6 or 20 mg/kg Xenon-45 PO formulated as previously described. Three or seven hours after the final dose, animals were euthanized to evaluate

compound levels in plasma and to monitor sebocyte viability. Animals were weighed daily and tumors measured with calipers twice weekly. Tumor volume was calculated according to the formula: Volume = (Length x Width^2 x Pi)/6. We used the Grubbs' test ($p<0.0001$) to eliminate one outlier in a mouse harboring a xenograft tumor derived from H2122 cells in Supplementary Fig. 6f (lower panel). Weight loss was less than 15% for twice daily dosing with 25 mg/kg SW203668, up to 7% with once daily Xenon-45 and negligible (<2%) for all other treatment groups.

Tissue harvest and histology preparation

Tissues for routine histology and special stains were harvested from anesthetized mice, were grossly trimmed, and then were immersion fixed in twenty-volumes of 10% neutral-buffered formalin. Following 48-hours of constant agitation in fixative, tissues were briefly rinsed and then dehydrated, cleared, and paraffin embedded by standard procedures[46,47]. Resulting embeds were sectioned on Leica RM2255 rotary microtomes at 5 μm thickness and subsequently stained by routine hematoxylin and eosin. All histology services were performed by members of the Molecular Pathology Core at UT Southwestern.

Microscopy

Review and photography of histologic preparations were carried out on a Leica DM2000 photomicroscope equipped with bright-field illumination. Photomicrography was achieved using this microscope and an Optronics Microfire digital CCD color camera interfaced with Macintosh G4 computer. Images were captured using PictureFrame 2.0 acquisition software (Optronics, Inc. Goleta, CA, USA).

Supplementary Material

Refer to Web version on PubMed Central for supplementary material.

Acknowledgments

We thank Sivaramakrishna Yadavalli and David C. Trudgian for advice on proteomics, David W. Russell for guidance on biochemical assays of sebaceous glands and preputial gland dissection, Jeffrey G. McDonald and Matthew Mitsche for advice on fatty acid flux analyses and Steven L. McKnight for helpful discussions and suggestions on the manuscript. CRN acknowledges the Clayton Foundation for Research and National Institutes of Health grant HL20948 for support. HM acknowledges the Cancer Prevention Research Institute of Texas (CPRIT) (RP120613) for funding. BAP acknowledges the Simmons Cancer Center (NCI 1P30CA142543-01), CPRIT (RP110708-C2) and CTD2 (1 U01 CA176284-01) for funding. NSW acknowledges CPRIT (RP110708-C3) for funding. JMR acknowledges CPRIT (RP110708-P3) and the Welch Foundation (I-1612) for funding. DN acknowledges the Disease Oriented Clinical Scholar (DOCS) award, the Presidential Research Council (PRC) award, the Welch Foundation (I-1879) and the Damon Runyon Clinical Investigator Award.

References

1. Rodriguez-Antona C, Ingelman-Sundberg M. Cytochrome P450 pharmacogenetics and cancer. Oncogene. 2006; 25:1679–1691. DOI: 10.1038/sj.onc.1209377 [PubMed: 16550168]
2. Estabrook RW. The remarkable P450s: a historical overview of these versatile hemeprotein catalysts. FASEB journal: official publication of the Federation of American Societies for Experimental Biology. 1996; 10:202–204. [PubMed: 8641552]

3. Rainov NG, et al. New prodrug activation gene therapy for cancer using cytochrome P450 4B1 and 2-aminoanthracene/4-ipomeanol. Human gene therapy. 1998; 9:1261–1273. DOI: 10.1089/hum.1998.9.9-1261 [PubMed: 9650611]
4. Doloff JC, Waxman DJ. Adenoviral vectors for prodrug activation-based gene therapy for cancer. Anti-cancer agents in medicinal chemistry. 2014; 14:115–126. [PubMed: 23869779]
5. Rowinsky EK, et al. Phase I and pharmacological study of the pulmonary cytotoxin 4-ipomeanol on a single dose schedule in lung cancer patients: hepatotoxicity is dose limiting in humans. Cancer research. 1993; 53:1794–1801. [PubMed: 8467498]
6. Slaughter SR, Statham CN, Philpot RM, Boyd MR. Covalent binding of metabolites of 4-ipomeanol to rabbit pulmonary and hepatic microsomal proteins and to the enzymes of the pulmonary cytochrome P-450-dependent monooxygenase system. The Journal of pharmacology and experimental therapeutics. 1983; 224:252–257. [PubMed: 6848746]
7. Miyazaki M, et al. Hepatic stearoyl-CoA desaturase-1 deficiency protects mice from carbohydrate-induced adiposity and hepatic steatosis. Cell metabolism. 2007; 6:484–496. DOI: 10.1016/j.cmet.2007.10.014 [PubMed: 18054317]
8. Corp. MSD. Pharmacokinetics and Pharmacodynamics of MK-8245 in Participants With Type 2 Diabetes (MK-8245-012). 2009. <https://clinicaltrials.gov/ct2/show/results/NCT00972322>
9. Ackerman D, Simon MC. Hypoxia, lipids, and cancer: surviving the harsh tumor microenvironment. Trends in cell biology. 2014; 24:472–478. DOI: 10.1016/j.tcb.2014.06.001 [PubMed: 24985940]
10. Paton CM, Ntambi JM. Biochemical and physiological function of stearoyl-CoA desaturase. American journal of physiology. Endocrinology and metabolism. 2009; 297:E28–37. DOI: 10.1152/ajpendo.90897.2008 [PubMed: 19066317]
11. Listenberger LL, et al. Triglyceride accumulation protects against fatty acid-induced lipotoxicity. Proceedings of the National Academy of Sciences of the United States of America. 2003; 100:3077–3082. DOI: 10.1073/pnas.0630588100 [PubMed: 12629214]
12. Hess D, Chisholm JW, Igal RA. Inhibition of stearoylCoA desaturase activity blocks cell cycle progression and induces programmed cell death in lung cancer cells. PloS one. 2010; 5:e11394. [PubMed: 20613975]
13. Scaglia N, Igal RA. Inhibition of Stearoyl-CoA Desaturase 1 expression in human lung adenocarcinoma cells impairs tumorigenesis. International journal of oncology. 2008; 33:839–850. [PubMed: 18813799]
14. Mason P, et al. SCD1 inhibition causes cancer cell death by depleting mono-unsaturated fatty acids. PloS one. 2012; 7:e33823. [PubMed: 22457791]
15. Roongta UV, et al. Cancer cell dependence on unsaturated fatty acids implicates stearoyl-CoA desaturase as a target for cancer therapy. Molecular cancer research: MCR. 2011; 9:1551–1561. DOI: 10.1158/1541-7786.MCR-11-0126 [PubMed: 21954435]
16. Zhang Z, Dales NA, Winther MD. Opportunities and challenges in developing stearoyl-coenzyme A desaturase-1 inhibitors as novel therapeutics for human disease. Journal of medicinal chemistry. 2014; 57:5039–5056. DOI: 10.1021/jm401516c [PubMed: 24295027]
17. Meingassner JG, et al. Pharmacological inhibition of stearoyl CoA desaturase in the skin induces atrophy of the sebaceous glands. The Journal of investigative dermatology. 2013; 133:2091–2094. DOI: 10.1038/jid.2013.89 [PubMed: 23446987]
18. Cheng JB, Russell DW. Mammalian wax biosynthesis. II. Expression cloning of wax synthase cDNAs encoding a member of the acyltransferase enzyme family. The Journal of biological chemistry. 2004; 279:37798–37807. DOI: 10.1074/jbc.M406226200 [PubMed: 15220349]
19. Kim HS, et al. Systematic identification of molecular subtype-selective vulnerabilities in non-small-cell lung cancer. Cell. 2013; 155:552–566. DOI: 10.1016/j.cell.2013.09.041 [PubMed: 24243015]
20. Ramirez RD, et al. Immortalization of human bronchial epithelial cells in the absence of viral oncoproteins. Cancer research. 2004; 64:9027–9034. DOI: 10.1158/0008-5472.CAN-04-3703 [PubMed: 15604268]
21. Kolb HC, Finn MG, Sharpless KB. Click Chemistry: Diverse Chemical Function from a Few Good Reactions. Angewandte Chemie. 2001; 40:2004–2021. [PubMed: 11433435]

22. Zhang L, Ge L, Parimoo S, Stenn K, Prouty SM. Human stearoyl-CoA desaturase: alternative transcripts generated from a single gene by usage of tandem polyadenylation sites. The Biochemical journal. 1999; 340(Pt 1):255–264. [PubMed: 10229681]
23. Liu G, et al. Discovery of potent, selective, orally bioavailable stearoyl-CoA desaturase 1 inhibitors. Journal of medicinal chemistry. 2007; 50:3086–3100. DOI: 10.1021/jm070219p [PubMed: 17530838]
24. Talamo BR, Bloch K. A new assay for fatty acid desaturation. Analytical biochemistry. 1969; 29:300–304. [PubMed: 5792566]
25. Hukkanen J, Pelkonen O, Hakkola J, Raunio H. Expression and regulation of xenobiotic-metabolizing cytochrome P450 (CYP) enzymes in human lung. Critical reviews in toxicology. 2002; 32:391–411. DOI: 10.1080/20024091064273 [PubMed: 12389869]
26. Leclerc J, et al. Profiling gene expression of whole cytochrome P450 superfamily in human bronchial and peripheral lung tissues: Differential expression in non-small cell lung cancers. Biochimie. 2010; 92:292–306. DOI: 10.1016/j.biochi.2009.12.007 [PubMed: 20034539]
27. Barretina J, et al. The Cancer Cell Line Encyclopedia enables predictive modelling of anticancer drug sensitivity. Nature. 2012; 483:603–607. DOI: 10.1038/nature11003 [PubMed: 22460905]
28. Miyata N, et al. HET0016, a potent and selective inhibitor of 20-HETE synthesizing enzyme. British journal of pharmacology. 2001; 133:325–329. DOI: 10.1038/sj.bjp.0704101 [PubMed: 11375247]
29. Zhang Z, et al. Discovery of piperazin-1-ylpyridazine-based potent and selective stearoyl-CoA desaturase-1 inhibitors for the treatment of obesity and metabolic syndrome. Journal of medicinal chemistry. 2013; 56:568–583. DOI: 10.1021/jm301661h [PubMed: 23245208]
30. Cerami E, et al. The cBio cancer genomics portal: an open platform for exploring multidimensional cancer genomics data. Cancer discovery. 2012; 2:401–404. DOI: 10.1158/2159-8290.CD-12-0095 [PubMed: 22588877]
31. Flowers MT, Ade L, Strable MS, Ntambi JM. Combined deletion of SCD1 from adipose tissue and liver does not protect mice from obesity. Journal of lipid research. 2012; 53:1646–1653. DOI: 10.1194/jlr.M027508 [PubMed: 22669918]
32. Dhar M, Sepkovic DW, Hirani V, Magnusson RP, Lasker JM. Omega oxidation of 3-hydroxy fatty acids by the human CYP4F gene subfamily enzyme CYP4F11. Journal of lipid research. 2008; 49:612–624. DOI: 10.1194/jlr.M700450-JLR200 [PubMed: 18065749]
33. Shanklin J, Guy JE, Mishra G, Lindqvist Y. Desaturases: emerging models for understanding functional diversification of diiron-containing enzymes. The Journal of biological chemistry. 2009; 284:18559–18563. DOI: 10.1074/jbc.R900009200 [PubMed: 19363032]
34. Fox BG, Lyle KS, Rogge CE. Reactions of the diiron enzyme stearoyl-acyl carrier protein desaturase. Accounts of chemical research. 2004; 37:421–429. DOI: 10.1021/ar030186h [PubMed: 15260504]
35. Hardwick JP. Cytochrome P450 omega hydroxylase (CYP4) function in fatty acid metabolism and metabolic diseases. Biochemical pharmacology. 2008; 75:2263–2275. DOI: 10.1016/j.bcp.2008.03.004 [PubMed: 18433732]
36. Wang H, et al. Crystal structure of human stearoyl-coenzyme A desaturase in complex with substrate. Nature structural & molecular biology. 2015; 22:581–585. DOI: 10.1038/nsmb.3049
37. Bai Y, et al. X-ray structure of a mammalian stearoyl-CoA desaturase. Nature. 2015
38. Trudgian DC, et al. CPFP: a central proteomics facilities pipeline. Bioinformatics. 2010; 26:1131–1132. DOI: 10.1093/bioinformatics/btq081 [PubMed: 20189941]
39. Craig R, Beavis RC. TANDEM: matching proteins with tandem mass spectra. Bioinformatics. 2004; 20:1466–1467. DOI: 10.1093/bioinformatics/bth092 [PubMed: 14976030]
40. Geer LY, et al. Open mass spectrometry search algorithm. Journal of proteome research. 2004; 3:958–964. DOI: 10.1021/pr0499491 [PubMed: 15473683]
41. Elias JE, Gygi SP. Target-decoy search strategy for increased confidence in large-scale protein identifications by mass spectrometry. Nature methods. 2007; 4:207–214. DOI: 10.1038/nmeth1019 [PubMed: 17327847]

42. Quehenberger O, Armando AM, Dennis EA. High sensitivity quantitative lipidomics analysis of fatty acids in biological samples by gas chromatography-mass spectrometry. Biochimica et biophysica acta. 2011; 1811:648–656. DOI: 10.1016/j.bbalip.2011.07.006 [PubMed: 21787881]

43. Morselli E, et al. Hypothalamic PGC-1alpha protects against high-fat diet exposure by regulating ERalpha. Cell reports. 2014; 9:633–645. DOI: 10.1016/j.celrep.2014.09.025 [PubMed: 25373903]

44. Moffat J, et al. A lentiviral RNAi library for human and mouse genes applied to an arrayed viral high-content screen. Cell. 2006; 124:1283–1298. DOI: 10.1016/j.cell.2006.01.040 [PubMed: 16564017]

45. McNaney CA, et al. An automated liquid chromatography-mass spectrometry process to determine metabolic stability half-life and intrinsic clearance of drug candidates by substrate depletion. Assay and drug development technologies. 2008; 6:121–129. DOI: 10.1089/adt.2007.103 [PubMed: 18336089]

46. Shehan, DCaHBB. Theory and Practice of Histotechnology. 2. Battelle Press; 1980.

47. Woods, AEaERC. Laboratory Histopathology, A Complete Reference. Churchill – Livingston Press; 1996.

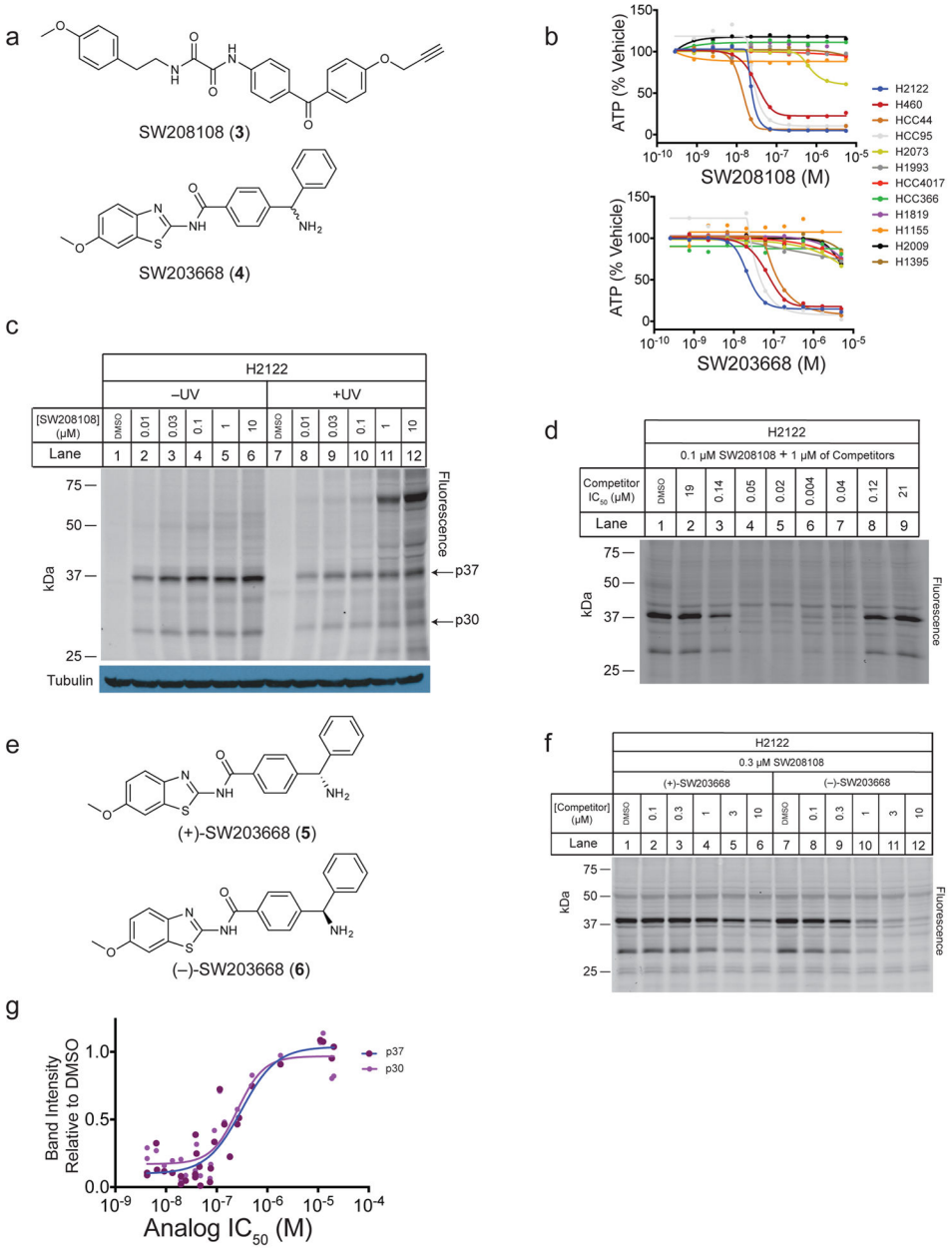

Figure 1.

Oxalamides and benzothiazoles are selective toxins identified in a high throughput small molecule phenotypic screen that target the same proteins. a. Chemical structures of the optimized oxalamide probe, SW208108, and the optimized bioavailable benzothiazole, SW203668. b. Concentration-response toxicity curves across a panel of 12 NSCLC cell lines. Each point represents the average of two biological replicates. c. SW208108 cross-linking to proteins in H2122, a sensitive cell line. Lysates were clicked to Alexafluor 532-azide (synthesis described in the Supplementary Chemical Procedures) in order to visualize bound proteins by fluorescence. Full gel is shown in Supplementary Fig. 1n. d. Competition of SW208108 with a panel of oxalamide analogues of varying potency. Non-specific band at

approximately 40kDa indicates equal sample loading. Full gel is shown in Supplementary Fig. 1o. e. Chemical structures of benzothiazole enantiomers (+)-SW203668 and (−)-SW203668 (H2122 IC_{50} values: 0.029 μM and 0.007 μM, respectively). f. Competition of oxalamide SW208108 with the benzothiazole enantiomers. Non-specific band at approximately 50kDa indicates equal sample loading. Full gel is shown in Supplementary Fig. 1p. g. Correlation of quantified competition to potency of a panel of 30 oxalamide and benzothiazole analogues. Each point represents one replicate. The corresponding gels are shown in figure 1d and supplementary figure 1f.

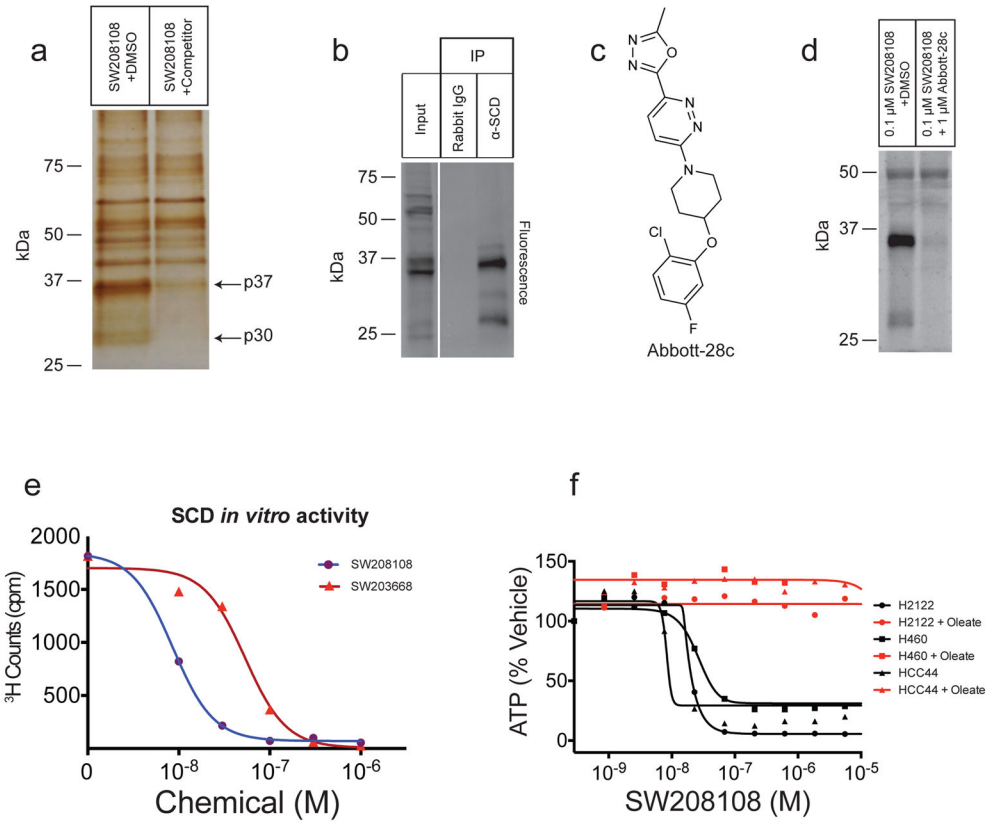

Figure 2.

Stearoyl CoA desaturase-1 (SCD) is the target of the oxalamides and benzothiazoles. a. Silver stain of purified p37 and p30 proteins. H2122 cells were treated with SW208108 with or without 3 μM (−)-SW203668, an active competitor. Full gel image is shown in Supplementary Figure 2a. b. Immunoprecipitation of SCD from 0.1 μM SW208108-treated H2122 cell lysate following conjugation of a fluorescent azide. Full gel is shown in Supplementary Figure 2b. c. Structure of known SCD inhibitor, Abbott-28c. d. Competition of SW208108 with Abbott-28c. Full gel image is shown in Supplementary Figure 2c. e. *In vitro* inhibition of SCD activity by oxalamide and benzothiazole scaffolds in microsomal preparation of H2122 cells. Each data point represents one replicate. Counts shown are after subtraction of counts from a control sample lacking NADPH. f. Rescue of oxalamide toxicity by 100 μM of sodium oleate. Each point represents the average of two biological replicates. Best fit curves of H460 + oleate and HCC44 + oleate are overlapping.

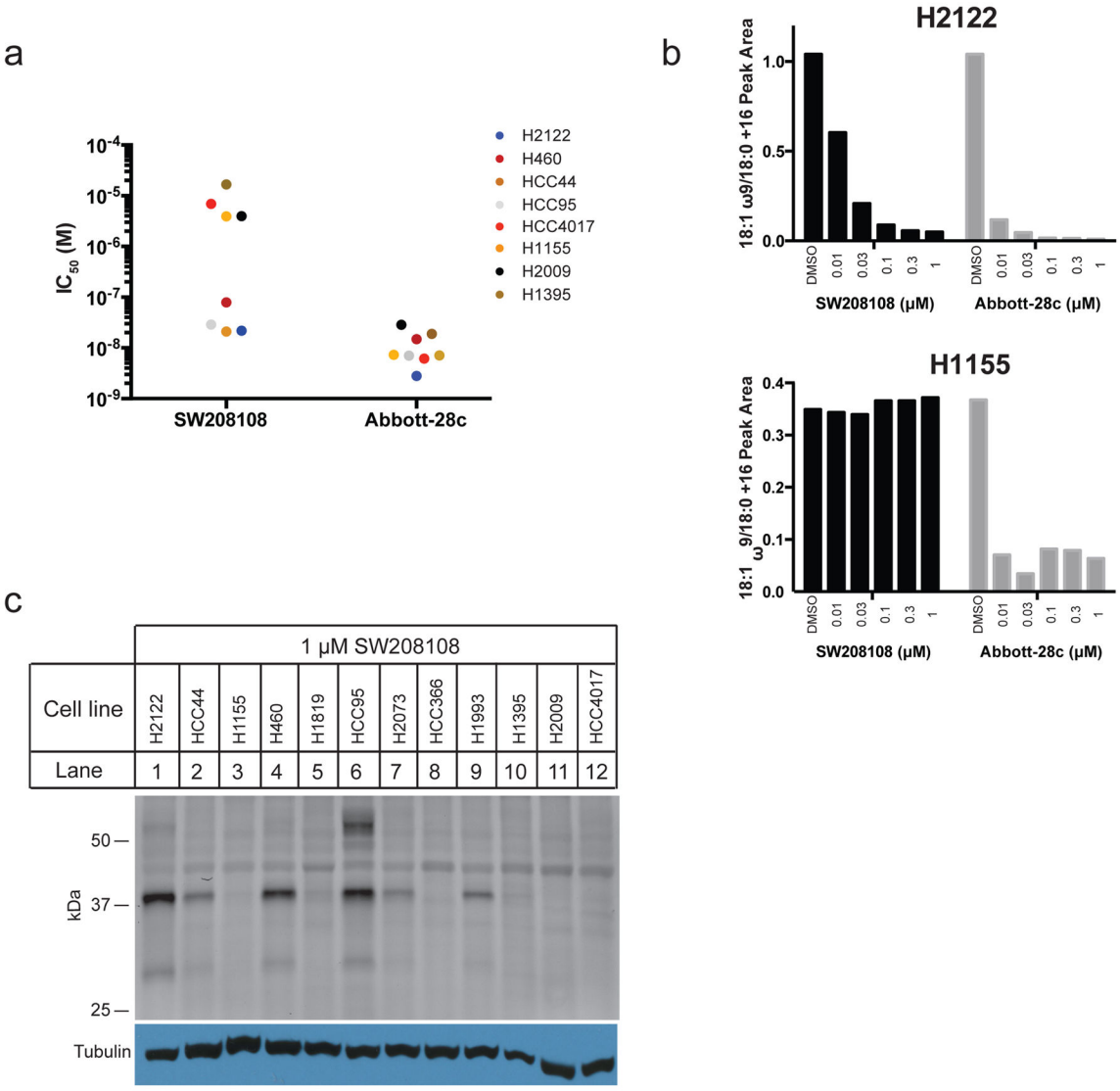

Figure 3.

Known SCD inhibitors are non-selectively toxic to cancer cell lines, while oxalamides are selectively toxic. a. Selectivity of oxalamide SW208108 and a known SCD inhibitor, Abbott-28c, in a panel of eight NSCLC lines. b. Measurements of the conversion of palmitate to oleate, which reflects SCD activity, in the presence of SW208108 or Abbott-28c in H2122 and H1155 cell lines. Each bar represents one replicate. c. Cross-linking of SW208108 in the panel of 12 NSCLC cell lines. Full gel image is shown in Supplementary Figure 3c.

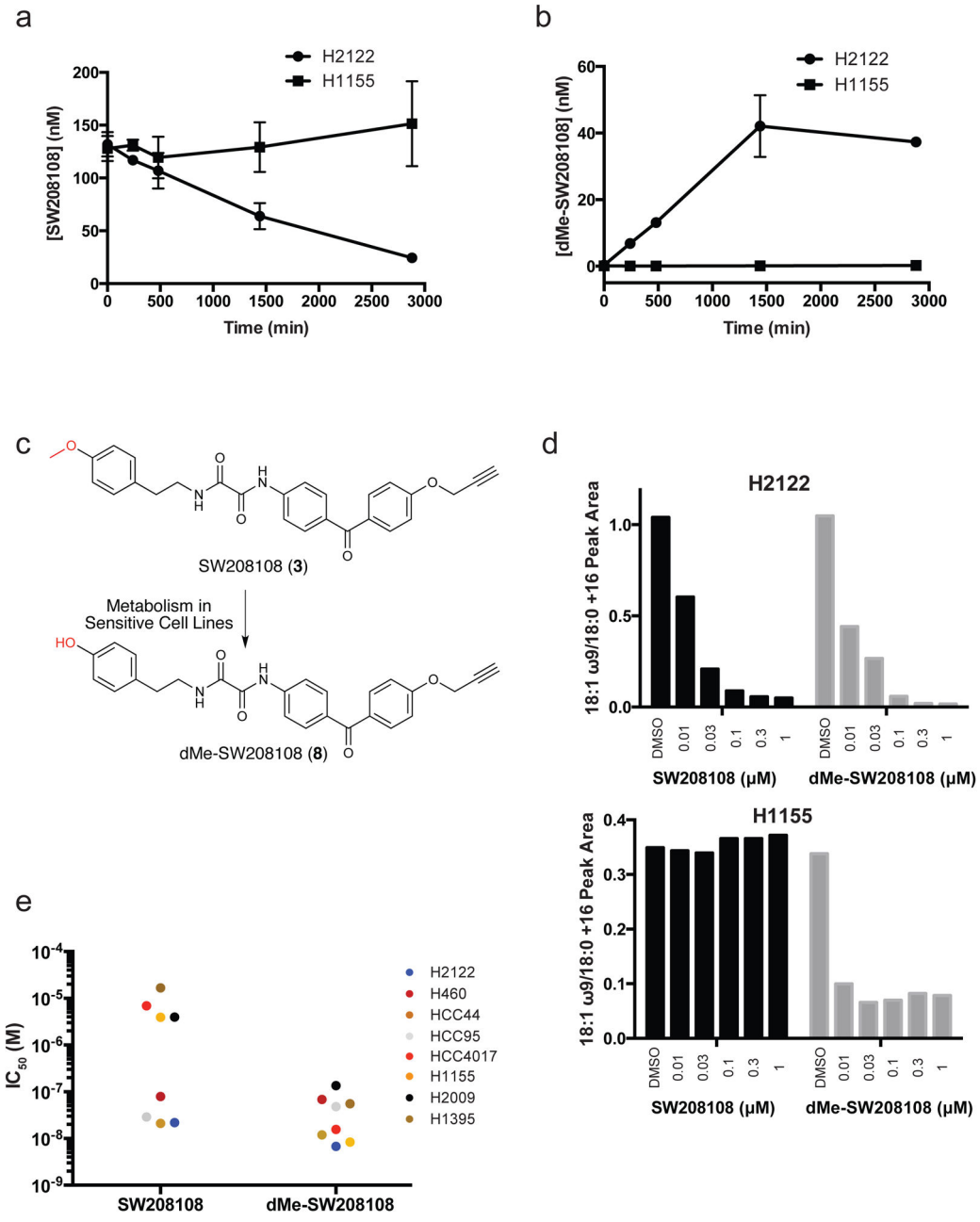

Figure 4.

Oxalamides inhibit SCD only in sensitive lines. They are pro-drugs that are selectively demethylated in sensitive lines to produce a non-selective SCD inhibitor. a. Levels of SW208108 in the presence of sensitive (H2122) and insensitive (H1155) cell lines. Error bars are plotted for all data points and represent standard deviation (n=3 biological replicates). b. Levels of de-methylated SW208108 (dMe-SW208108) in the above two lines after treatment with SW208108. Error bars represent standard deviation (n=3 biological replicates). c. Metabolism of oxalamide that occurs in the sensitive cell lines. d. Fatty acid flux through SCD in the above two cell lines in the presence of SW208108 or dMe-

SW208108. Each bar represents one replicate. Data for SW208108 is re-shown from Fig. 3b.

e. Selectivity of SW208108 and its demethylated metabolite across a panel of eight cell lines. Data for SW208108 is re-shown from Fig. 3a.

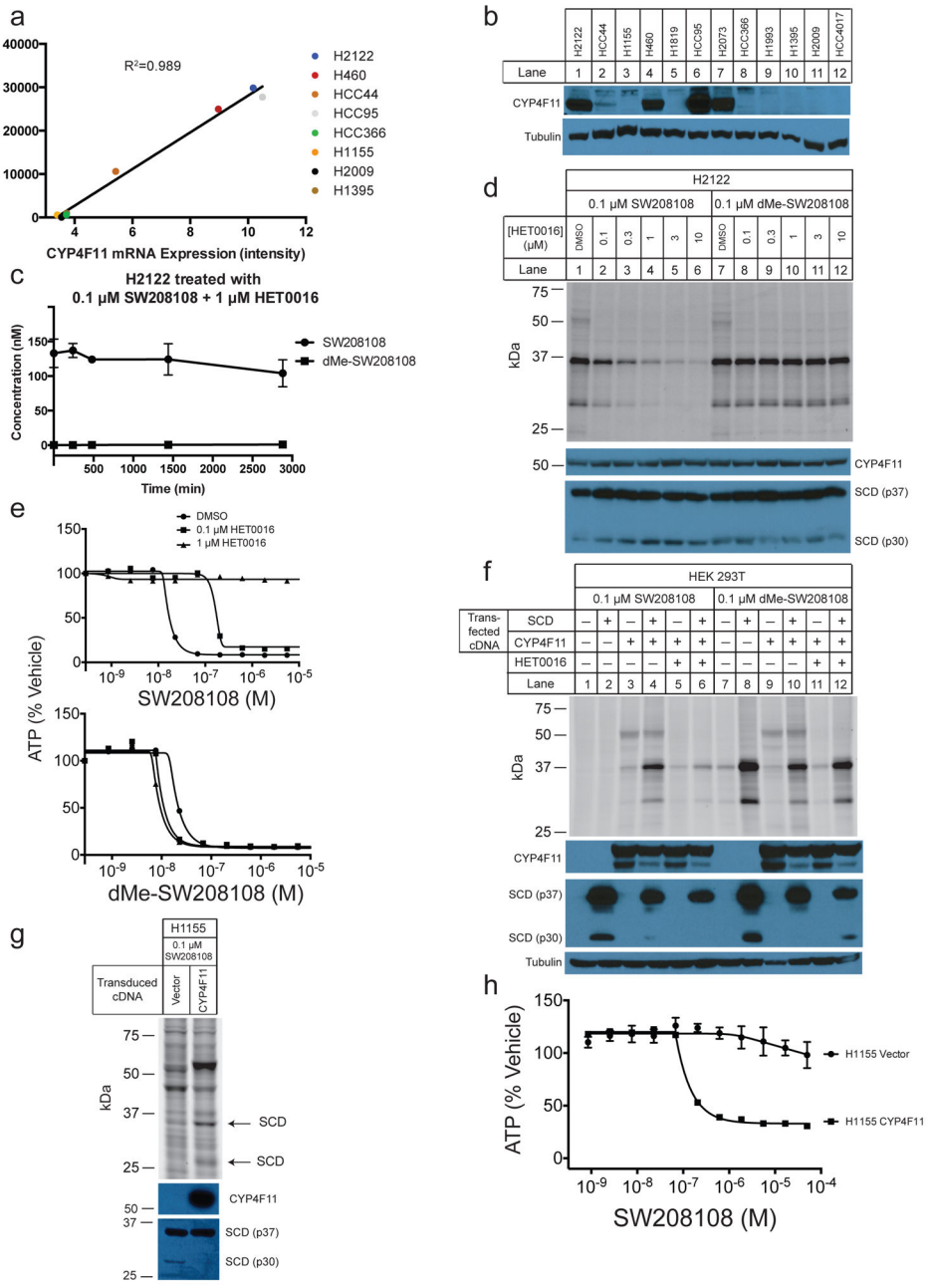

Figure 5.

Cytochrome P450 4F11 (CYP4F11) is responsible for oxalamide activation in sensitive cell lines and it is not expressed in insensitive cell lines. a. Correlation of CYP4F11 mRNA levels in a panel of eight cell lines to the quantitated intensity of SW208108 cross-linked SCD that is shown in Fig. 3c. b. CYP4F11 levels across the panel of 12 NSCLC lines using the same samples initially shown in figure 3c. Full gel image is shown in Supplementary Figure 5f. The levels of tubulin are also reshown to demonstrate equal loading. c. Effect of a known CYP4F11 inhibitor, HET0016, on SW208108 metabolism in a sensitive line, H2122. Errors represent standard deviation (n=3 biological replicates). d. Inhibition of SW208108

cross-linking to SCD by HET0016. Full gel image is shown in Supplementary Figure 5g. e. HET0016 rescues H2122 cells from toxicity to SW208108 (pro-drug) but not dMe-SW208108 (drug). Each point represents the average of two biological replicates. f. Reconstitution of CYP4F11-dependent SW208108 cross-linking to SCD in HEK293T cells. Full gel image is shown in Supplementary Figure 5h. g. Stable expression of CYP4F11 in an insensitive line, H1155, and resultant cross-linking of SW208108. Full gel image is shown in Supplementary Figure 5i. h. Oxalamide pro-drug, SW208108, concentration response curve of H1155-vector or CYP4F11 infected cell. Each point represents the average of two biological replicates.

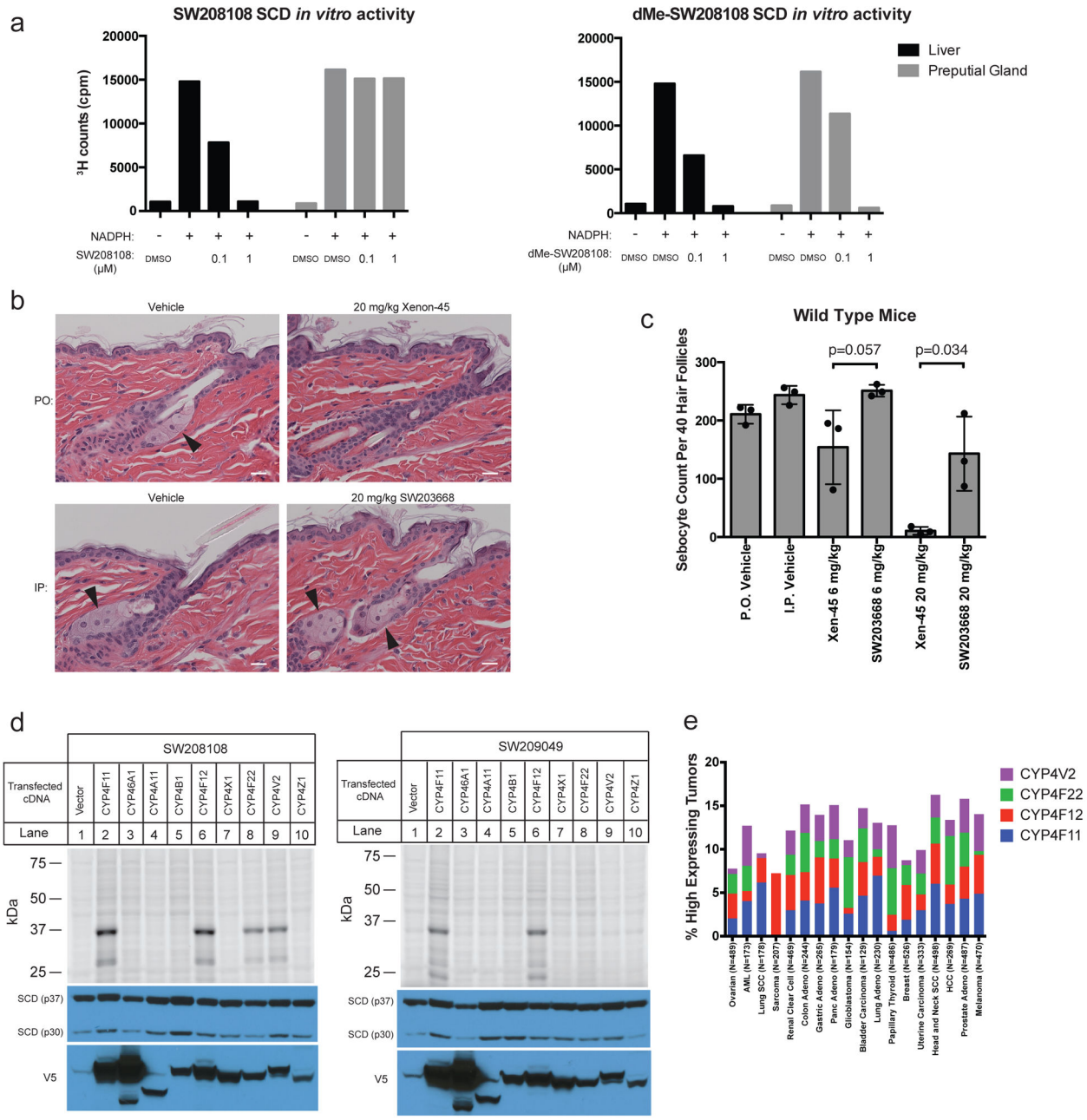

Figure 6.

The CYP-activated SCD inhibitors are not activated by sebaceous glands and display a therapeutic window to avoid sebaceous gland toxicity compared to known SCD inhibitors. a. *Ex vivo* inhibition of SCD by oxalamide pro-drug SW208108 and active species dMe-SW208108 in wild type mouse liver and sebaceous (preputial) gland microsomes. Each bar represents one replicate. b. Hematoxylin and eosin stained skin sections of wild type mice treated with a known bioavailable SCD inhibitor, Xenon-45, or benzothiazole SW203668 at 20 mg/kg for two weeks, once daily dosing. Arrowheads indicate sebocytes. Scale bars represent 20 μm. c. Quantitation of sebocytes in mouse skin sections of wild type mice

treated with 6 or 20 mg/kg for 2 weeks (one-tailed t-test). Error bars represent standard deviation (n=3 biological replicates). d. Oxalamide probe, SW208108, (left) and benzothiazole probe, SW209049, (right) cross-linking in HEK293T cells over-expressing a panel of nine type 4 CYP enzymes. Full gel images are shown in Supplementary Figure 6h. e. Percentage of cancers expressing high levels of the CYP4 family that activate the oxalamides and benzothiazoles. SCC refers to squamous cell carcinoma and HCC refers to hepatocellular carcinoma.